Hydrol. Earth Syst. Sci. Discuss., 10, 12615–12641, 2013
www.hydrol-earth-syst-sci-discuss.net/10/12615/2013/
doi:10.5194/hessd-10-12615-2013

Hydrology and Earth System Sciences Discussions
Open Access

Analysis of an extreme rainfall-runoff event at the Landscape Evolution Observatory by means of a three-dimensional physically-based hydrologic model

G.-Y. Niu[1,2], D. Pasetto[3], C. Scudeler[3], C. Paniconi[3], M. Putti[4], and P. A. Troch[1,2]

[1]Biosphere 2, the University of Arizona, Tucson, USA
[2]Department of Hydrology and Water Resources, the University of Arizona, Tucson, USA
[3]Institut National de la Recherche Scientifique, Centre Eau Terre Environnement (INRS-ETE), Université du Québec, Quebec City, Canada
[4]Department of Mathematics, University of Padova, Padova, Italy

Received: 20 September 2013 – Accepted: 3 October 2013 – Published: 18 October 2013

Correspondence to: G.-Y. Niu (niug@email.arizona.edu)

Published by Copernicus Publications on behalf of the European Geosciences Union.

Abstract

We present a detailed analysis, by means of a three-dimensional physically-based hydrological model, of the first experiment conducted at the Biosphere 2 Landscape Evolution Observatory (LEO). The experiment was driven by an intense rainfall event and produced a hydrological response characterized predominantly by water outflow along the lower lateral boundary (seepage face) of LEO, together with overland flow that began 15 h after the start of rainfall and caused erosion of the superficial soil and formation of a small channel. The analysis is designed to test the null hypothesis that the soil is hydraulically homogenous, and an alternative hypothesis that the soil has developed some hydraulic heterogeneity in the downstream direction due to saturated soil compaction near the seepage face. More than 20 000 sensitivity simulations were run in a systematic search for optimal parameters to reproduce measurements of seepage face outflow and hillslope water storage. We varied the saturated hydraulic conductivity (K_{sat}) of the seepage face (18 values), K_{sat} in the rest of the LEO soil (30 values), and soil porosity (21 values), and we considered two values of the pore size distribution parameter (n) in the water retention characteristics, obtained from a particle size distribution analysis and from laboratory experiments on LEO soil samples. For both n values, the best simulations under the heterogeneous soil hypothesis produced smaller errors than the best runs under the null hypothesis. Moreover the heterogeneous runs yielded a higher probability of best realizations than the homogenous runs. These results support the hypothesis of localized incipient heterogeneity of the LEO soil.

1 Introduction

To improve predictive understanding of the coupled physical, chemical, biological, and geological processes at the Earth's surface in changing climates, the University of Arizona has constructed a large-scale and community-oriented research infrastructure – the Biosphere 2 Landscape Evolution Observatory (LEO) near Tucson, Arizona, USA.

The infrastructure is designed to facilitate investigation of emergent structural heterogeneity that results from coupled Earth surface processes. Feedbacks and interactions between different Earth surface processes are studied through iterations of experimental measurement and development of coupled, physically-based numerical models (Huxman et al., 2009). The controlled environment of LEO constitutes an ideal platform for validating and improving the models, and in turn the models can help interpret the measured data, corroborate and characterize the formation of soil and ecosystem heterogeneity, and design subsequent experiments.

LEO consists of three identical, 30 m long and 11.15 m wide, convergent landscapes. These landscapes are being studied in replicate as "bare soil" for an initial period of two to three years. During this time, investigations will focus on hydrological processes, surface modification by rainsplash and overland flow, hillslope-scale water transit times, evolution of moisture state distribution, rates and patterns of geochemical processes, emergent non-vascular and microbial ecology, and carbon and energy cycle dynamics within the shallow subsurface. Detailed hydrogeochemical modeling predicted that within three years of treatment, the basalt parent material will develop significant changes in subsurface structure, including pore size and particle size changes that could potentially affect hydrologic flow pathways (Dontsova et al., 2009). Accelerated co-evolution of the physical and biological systems is expected following introduction of heat- and drought-tolerant vascular plant communities.

The Biosphere 2 LEO has been constructed after a period of community-based scientific planning (Hopp et al., 2009; Dontsova et al., 2009; Ivanov et al., 2009). The first hillslope of LEO (LEO#1) was commissioned at the end of 2012, while the second and third hillslopes are expected to be completed by the fall of 2013. From 2014 on, all three hillslopes will be monitored simultaneously while experiencing a climate representative for the semi-arid southwest of the United States. Monitoring will include rain amounts and intensity, soil moisture and soil water potential spatio-temporal distributions, perched groundwater dynamics, seepage flow, surface runoff and associated solute and sediment transport out of the hillslope, and total mass storage changes.

HESSD
10, 12615–12641, 2013

Geochemical analysis of rain, soil, seepage, and surface runoff water and CO_2 analysis of soil air samples using embedded automatic sensors will complete routine monitoring procedures.

Between LEO#1 commissioning and the completion of the entire LEO (December 2012–September 2013) a series of stand-alone rainfall-runoff experiments were scheduled. These experiments were designed to reveal internal hydrologic and geochemical dynamics, to test sensor and sampler infrastructure across a wide range of wetness conditions, and to fine-tune data acquisition and processing software and hardware. The amount of water used during these experiments will be applied to the two other hillslopes to provide similar geochemical conditions before the parallel continuous long-term experiment starts in 2014. Simulations with uncoupled three-dimensional (3-D) hydrologic and solute transport models were run prior to the experiments to predict the hydrologic and water particle response.

The objective of the first experiment, which started at 10:00 LT on 18 February 2013, was to bring the hillslope to a hydrologic steady-state using a continuous and constant rain rate and observe how the hillslope internal states respond to this stepwise input. Numerical simulation had predicted that the hillslope would reach hydrologic steady-state after 24 h. The rain was scheduled to be turned off after steady-state to allow the hillslope to drain for a week after reaching steady-state, and then another continuous and constant rain event labeled with deuterium was planned. The second event would allow us to observe the difference between the flow and transport processes by comparing hydrologic response and the breakthrough curves of the tracer at different locations within and at the outlet of the hillslope. Automatic sampling of rain and seepage water was programmed at every 15 min, while manual sampling from a subset of the soil suction lysimeter array was attempted every three hours. Chemical analysis of these samples should inform us about water transit time distributions during the experiment as well as initial geochemical weathering rates and associated carbon sequestration.

The hillslope never reached the predicted steady-state but instead developed saturation excess overland flow, which transported 0.7 m^3 of soil and generated a shallow gully in the central trough of the hillslope. In this work we present an in-depth analysis of the observed hydrologic response to answer the question: why did the observed hydrological response differ so significantly from the predicted response? The analysis is based on pre- and post-experiment simulation results using a 3-D physically-based hydrological model. The investigation focuses on how overland flow was generated and on the important role of localized heterogeneity in overland flow generation. The soil hydraulic parameters are calibrated against measurements of total mass change and seepage face flow collected during the experiment. In addition, sensitivity analyses of the model outputs with respect to homogeneous and heterogeneous soils are conducted to search for optimal soil parameters over a wider parameter space.

2 Methodology

2.1 Biosphere 2 Landscape Evolution Observatory (LEO)

LEO consists of three identical, sloping (10 degree on average), 334.5 m^2 convergent landscapes inside a 5000 m^2 environmentally controlled facility (Fig. 1). These engineered landscapes contain 1 m depth of basaltic tephra ground to homogenous loamy sand that will evolve into structured soil over the years. Each landscape contains a spatially dense sensor and sampler network capable of resolving meter-scale lateral heterogeneity and sub-meter scale vertical heterogeneity in moisture, energy, and carbon states and fluxes. The density of sensors and frequency at which they can be polled allows for measurements that are impossible to take in natural field settings. Embedded soil water solution and soil gas samplers allow for quantification of biogeochemical processes, and they facilitate the use of chemical tracers at very dense spatial scales to study water movement. Each ~ 1 000 000 kg landscape has load cells embedded into the structure to measure changes in total system mass weight with 0.05 % full-

HESSD
10, 12615–12641, 2013

scale repeatability (equivalent to less than 1 cm of precipitation). Each landscape has an engineered rain system that allows application of precipitation at rates between 3 and 45 mm h^{-1} in spatially homogeneous or heterogeneous patterns, and with enough capability to produce hillslope scale hydrological steady-state conditions or to run complex hyetograph simulations. The precipitation water supply storage system is flexibly designed to facilitate addition of tracers in constant or time-varying rates to any of the three hillslopes.

2.2 The hydrological model

We use the CATHY (CATchment HYdrology) model (Camporese et al., 2010) to simulate the partitioning of rainfall between runoff and infiltration, the subsurface redistribution of soil moisture and groundwater, and the discharge through the LEO seepage face. The subsurface flow module solves the 3-D Richards equation describing flow in variably saturated porous media while the surface flow module solves the diffusion wave equation describing surface flow propagation over hillslopes and in stream channels identified using terrain topography and the hydraulic geometry concept. Surface/subsurface coupling is based on a boundary condition switching procedure that automatically partitions potential fluxes (rainfall and evapotranspiration) into actual fluxes across the land surface and calculates changes in surface storage.

2.3 The first LEO experiment

The hydrological experiments on the first completed hillslope started at 10:00 LT, 18 February 2013 and ended at 08:00 LT, 19 February 2013. Rainfall at ~ 12 mm h^{-1} (4.01 m^3 h^{-1} in Fig. 2a) for a duration of 22 h produced an input of ~ 264 mm into the 1.0 m-deep soil of LEO with an initial water storage of 108 mm (36.13 m^3 in Fig. 2b). This experiment was designed to (1) test the functionality of all sensors, (2) investigate LEO's hydrological response under a heavy rainfall, and (3) generate a steady state of soil moisture for further tracer experiments. Prior to the experiment, we used CATHY to estimate the time for LEO to reach an equilibrium state under a constant precipitation rate: with the first calibration of the model, the seepage face outflow equaled the imposed precipitation rate after 1.5 d and no overland flow was predicted (see Sect. 2.4 for model configuration M1 and Sect. 3 for the results). However, in the actual experiment the response of LEO to the imposed precipitation drastically differed from what was predicted with CATHY. In fact, overland flow occurred 15 h after the start of rainfall, resulting in erosion of the superficial soil layers and the formation of a surface channel. Total mass change, total seepage flow, and soil moisture at 496 locations were recorded every 15 min during the experiment. An estimation of the overland flow and soil evaporation rates was achieved from the closure of water balance and volumetric flow measurements.

Figure 2 shows the hydrological data collected during the experiment. Time "0" corresponds to 08:00 LT 18 February (i.e., 2 h before the start of rainfall). Overland flow (Fig. 2d) reached a peak of about 1.8 $m^3 h^{-1}$ around 08.00 LT 19 February when the rain system was turned off. The maximum seepage face flow occurred about one hour later, with a magnitude of about 0.7 $m^3 h^{-1}$.

2.4 Model setup

We discretized the 30 m × 11.15 m × 1 m LEO soil into 60 × 24 grid cells (61 × 25 nodes) in the lateral direction and 8 layers (9 nodes) in the vertical direction (Fig. 3), assigning a higher resolution (0.05 m) to the surface and bottom layers to better resolve infiltration at the soil surface and seepage flow at the bottom nodes of the seepage face. We set up a seepage face boundary condition at the 25 × 8 downslope lateral boundary nodes of LEO (the 25 nodes along the surface edge of this lateral boundary were excluded; these nodes, together with all other nodes on the LEO surface, were assigned atmospheric boundary conditions). Aside from the seepage face and the land surface, all other LEO boundaries were set to a zero flux condition.

Because of the lack of direct measurements of soil surface evaporation (E), the atmospheric boundary condition (Q_{atm}) of the model was estimated separately for three

HESSD
10, 12615–12641, 2013

phases. During the daytime period from 08:00 to 20:00 LT of 18 February (time 0–12 h in Fig. 2a), E is not negligible. Q_{atm} was therefore estimated as the rate of change in total water storage ($\mathrm{d}S/\mathrm{d}t$) as measured by the load cell because the mass balance can be expressed as $\mathrm{d}S/\mathrm{d}t = P - E$, where P is rainfall, prior to the occurrence of major seepage face flow and overland flow. During the nighttime until the next morning when the rainfall stopped (time 12–24 h in Fig. 2a), E was assumed to be negligible, and Q_{atm} was thus set to the sprinkler rainfall rate ($\sim 12\,\text{mm}\,\text{h}^{-1}$). During the final phase after time 24 h with no rain, Q_{atm} was estimated at $-2\,\text{mm}\,\text{d}^{-1}$, where $2\,\text{mm}\,\text{d}^{-1}$ is the average evaporation rate from a wet surface for a winter month in Arizona.

Time stepping in the CATHY model is adaptive (based on the convergence of the iterative scheme used to linearize Richards' equation) and was set such that time step sizes ranged from 0.1 to 180 s. The convergence criterion on soil water pressure was set for a model accuracy of 1.0×10^{-3} m.

We designed six scenarios of numerical simulations taking into account different configurations of model parameters characterizing the soil properties, including the van Genuchten curve fitting parameter (n), the porosity (θ_{sat}), and the saturated hydraulic conductivity (K_{sat}). The scenarios and corresponding model parameter values are summarized in Table 1.

Scenarios M1 and M2 correspond to the numerical simulations performed before the physical experiment. M1 uses soil property parameters from an analysis of soil particle size distribution ($n = 2.26$, $\theta_{\text{sat}} = 0.39$, and $K_{sat} = 7.8 \times 10^{-6}\,\text{m}\,\text{s}^{-1}$). M2 uses the same parameters except for a greater K_{sat} ($= 3.8 \times 10^{-3}\,\text{m}\,\text{s}^{-1}$) resulting from a calibration against the timing of the measured seepage face flow of a pre-experiment with $20\,\text{mm}\,\text{h}^{-1}$ of rainfall for a duration of 5 h conducted in November 2012.

To generate overland flow it was found that the numerical model of LEO requires a lower soil porosity than the one used in M1 and M2 and/or a heterogeneous distribution of the hydraulic conductivity that slows down the seepage face outflow. Scenarios M3 and M4 are designed to assess the probability that K_{sat} at LEO's seepage face ($K_{\text{sat, sf}}$) may be less than that of the upslope soil and to search for the possible range of optimized parameters. M3 consists of two groups of experiments, one under the hypothesis of homogeneous soil (M3_Homo) and the other assuming that $K_{\text{sat, sf}}$ is less than the K_{sat} of the rest of the LEO soil (M3_Hetero). The values of the van Genuchten parameters n, ψ_{sat}, and θ_r used in scenario M3 were obtained by fitting the soil water retention data from laboratory experiments on the LEO soil samples (Fig. 4). In particular, for scenario M3 the value of n is 1.72. M3_Homo simulations were conducted with combinations of 21 values of θ_{sat} ranging from 0.33 to 0.38 at a step of 0.0025 and 30 values of K_{sat} ranging from 1 to $30 \times 10^{-5}\,\text{m}\,\text{s}^{-1}$ at a step of $1 \times 10^{-5}\,\text{m}\,\text{s}^{-1}$, for a total of 630 simulations. M3_Hetero further combines 18 values of $K_{\text{sat, sf}}$ ranging from $1.4 \times 10^{-5}\,\text{m}\,\text{s}^{-1}$ to $3.1 \times 10^{-5}\,\text{m}\,\text{s}^{-1}$ at a step of $1 \times 10^{-6}\,\text{m}\,\text{s}^{-1}$, for a total of $630 \times 18 = 11\,340$ simulations. Scenario M4 is analogous to scenario M3 except that $n = 2.26$, the same as in M1 and M2. This larger n value, estimated from a pre-experiment analysis of particle size distribution, tends to better match the in situ LEO data (Fig. 4), although there are uncertainties in the measurements.

To evaluate which set of parameter values allows us to best approximate the observed response amongst these several thousand model simulations, we computed the mean relative error between the measured and simulated data. For instance, let $\Delta S_{\text{m}(t)}$ and $\Delta S_{\text{s}(t)}$ be the measured and simulated variation of water storage at time t. We define the relative error $e_{\Delta S}$ as:

$$e_{\Delta S} = \frac{\int_0^T |\Delta S_\text{m} - \Delta S_\text{s}| \text{d}t}{\int_0^T \Delta S_\text{m}\, \text{d}t}. \tag{1}$$

The relative error for the seepage face flow (e_{QS}) is computed in the same way. The mean relative error is then defined as an average of the two:

$$e = \frac{1}{2}\left(e_{\Delta S} + e_{\text{QS}}\right). \tag{2}$$

We did not include the relative error of overland flow in the above averaged error because the observed response for this variable was derived from mass balance cal-

HESSD
10, 12615–12641, 2013

culations based on other measured variables. Its derivation also involves estimation of surface evaporation at later stages. Total water storage, on the other hand, was measured directly by means of 10 load cells, and seepage flow was also accurately measured by means of tipping bucket rain gauges and electromagnetic flow meters.

3 Modeling results

Figure 2 compares the modeling results from M1 and M2 to the measured overland flow, seepage face flow, and water storage. Neither M1 nor M2 produce any overland flow. Compared to the measured seepage face flow, M1 with its smaller K_{sat} ($7.8 \times 10^{-6}\,m\,s^{-1}$) produces negligible outflow at the seepage face, and therefore the modeled water storage stays at a constant value after it reaches its peak value. M2 on the other hand, with its much higher K_{sat} ($3.8 \times 10^{-3}\,m\,s^{-1}$) produces much higher outflow at the seepage face and lower water storage than the measured values. The M2 results indicate that the calibration of K_{sat} against the timing of the seepage face flow of the pre-experiment is misleading, because the LEO soil at this early stage may not have been well compacted, resulting in faster outflows at the seepage face. M1 and M2 produce seepage face flow and water storage that are very different from the measurements, and at opposite extremes. Since the modeled overland flow is zero for both cases, changes in K_{sat} are insufficient to retrieve the observed overland flow. We therefore conducted several sensitivity simulations to reduce θ_{sat} and/or $K_{sat,\,sf}$. These simulations helped produce overland flow and improved the simulation of seepage face flow and water storage, informing the design of the M3 and M4 experiments summarized in Figs. 5 and 6.

For scenario M3, Fig. 5 shows the relative model error across the parameter space of K_{sat} and θ_s for both the M3_Homo and M3_Hetero experiments. The results for M3_Hetero are obtained with $K_{sat,\,sf} = 2.1 \times 10^{-5}\,m\,s^{-1}$. M3_Hetero shows a relatively greater area of best simulations of seepage face flow (i.e., with relative errors at the low end that are smaller than 20 %) compared to M3_homo, for which the best results are concentrated along a narrow band around a K_{sat} value of 1.1×10^{-4} m s^{-1}. This suggests that M3_Hetero has a greater number of best simulations than M3_Homo. However, M3_Hetero shows a smaller area of best simulations of water storage with relative errors smaller than 10 % than does M3_Homo. In terms of the mean relative error combining the two response variables, M3_Hetero yields a larger number or greater probability of best simulations than M3_Homo. To clarify this point, in Fig. 7 we show a frequency analysis of the mean relative errors obtained in M3_Homo and M3_Hetero. The frequencies are normalized by the total number of simulations (630), so that the histograms are an approximation of the probability density functions (PDFs) of the mean errors. Taking relative error smaller than 15 % as a marker, M3_Hetero has more than 40 % best simulations compared with only 6 % for M3_Homo.

Similar results are obtained for scenario M4, where a value of 2.26 instead of 1.72 was set for parameter n. Figure 6 shows the comparison of M4_Homo and M4_Hetero simulations in terms of the relative errors across the parameter space of K_{sat} and θ_{sat}. The results for M4_Hetero are obtained with $K_{sat,\,sf} = 1.9 \times 10^{-5}$ m s^{-1}. M4_Hetero shows a larger area (or greater number) of best simulations than M4_Homo, more notably for seepage face flow. In terms of the mean relative error, M4_Hetero yields a greater probability of best simulations than M4_Homo. This is confirmed from the PDFs in Fig. 7, where M4_Hetero has about 16 % best simulations (taking relative error smaller than 10 % as a marker) while M4_Homo has only about 2 %. This implies that the assumption of $K_{sat,\,sf} < K_{sat}$ produces a greater probability of best realizations than that of $K_{sat,\,sf} = K_{sat}$, supporting the hypothesis of localized heterogeneity at the LEO hillslope.

Figure 7 also suggests that the overall performance of M4_Hetero is better than M3_Hetero. M4_Hetero produces 16 % best simulations with mean relative error smaller than 10 % whereas M3_Hetero produces none, while at the 15 % relative error level M4_Hetero yields a 50 % probability of best realizations compared to 42 % for M3_Hetero. In addition, the best simulation of M4_Hetero produces a smaller error (7.38 %) than that of M3_Hetero (10.74 %) (Table 2).

HESSD
10, 12615–12641, 2013

A further comparison between scenarios M3_Hetero and M4_Hetero is depicted in Fig. 8, which shows the PDFs of these two experiments across all 18 $K_{sat,\,sf}$ values and for three different values of mean relative error level (10, 15, and 20 %). When $K_{sat,\,sf} = 2.1 \times 10^{-5}\,m\,s^{-1}$, M3_Hetero reaches the greatest probability of best simulations with mean relative error less than 15 %, and when $K_{sat,\,sf} = 1.9 \times 10^{-5}\,m\,s^{-1}$, M4_Hetero reaches the greatest probability with relative error less than 10 %. M4_Hetero ($n = 2.26$) performs notably better than M3_Hetero ($n = 1.72$) over almost all the $K_{sat,\,sf}$ values (particularly at the 10 % error level).

The optimized $K_{sat,\,sf}$ values, corresponding to the best realizations out of the 11 340 simulations each of M3_Hetero and M4_Hetero, are, respectively, $2.3 \times 10^{-5}\,m\,s^{-1}$ and $2.2 \times 10^{-5}\,m\,s^{-1}$ (Table 2) (slightly larger than those corresponding to their greatest probabilities). These optimized values of $K_{sat,\,sf}$ coincidentally fall within the range of K_{sat} values obtained from the laboratory measurements ($1.9 \times 10^{-5} - 2.5 \times 10^{-5}\,m\,s^{-1}$) with the same soil (Hernandez and Schaap, 2012). The optimized K_{sat} values for the upslope are about 6.4 times greater than $K_{sat,\,sf}$ for M4_Hetero and 7.4 times greater for M3_Hetero. These modeling results thus once again support the hypothesis of localized heterogeneity at the lower end of LEO.

The modeled time series of seepage flow (Fig. 9b) from the best simulations of M3_Hetero and M4_Hetero explains why the best simulation prefers a greater n value. A greater n value produces a faster early response of outflow at the seepage face and more sustainable flow during the recession period. The optimized n value (2.26) is also consistent with the larger optimized K_{sat} value ($1.4 \times 10^{-4}\,m\,s^{-1}$), both suggesting a greater permeability of the LEO soil than that of the same soil in the laboratory (and at the seepage face).

As a result of calibration against seepage face flow and water storage, the best realizations for both M3_Hetero and M4_Hetero also produce a reasonable overland flow hydrograph, in phase with the hydrograph estimated from mass balance calculations though with a longer tail during the recession period (Fig. 9c). The modeled longer tail of overland flow may be induced by the uncertainty in the soil surface evaporation estimate ($2\,\mathrm{mm\,d^{-1}}$) used as the upper boundary condition during this period. With the large conductivity of the LEO soil (e.g., $K_{sat} = 1.4 \times 10^{-4}\,\mathrm{m\,s^{-1}}$ upslope of the seepage face for the optimal M4_Hetero simulation), the overland flow generation mechanism is saturation-excess (see also Gevaert et al., 2013), and therefore calibration of θ_{sat} and $K_{sat,\,sf}$ is critical for accurately reproducing this response. Figure 2 shows the degree of saturation of LEO when overland flow reaches its peak value. The water table first builds up at the lower end of LEO and then propagates upslope, with overland flow being triggered when the water table reaches the surface.

4 Discussion and conclusions

The first rainfall experiment with LEO#1 was designed to test the functionality of subsurface sensors and to generate hydrologic steady-state for system dynamics characterization and further tracer experiments. The design of this experiment in terms of rainfall intensity and duration was informed by hydrologic model simulations based on estimates of soil hydraulic properties. These model simulations predicted that the hillslope would reach steady-state in a reasonable amount of time (about 24 h) and that no overland flow through saturation excess would occur. The actual experiment resulted in saturated soils in the central trough of the hillslope that caused saturation excess overland flow and gully erosion. This study has explored possible reasons for the mismatch between model prediction and observations by performing numerous post-experiment model simulations within a much wider parameter space compared to the pre-experiment simulations.

Model simulations under homogeneous soil conditions, using soil parameters estimated from an analysis of particle size distribution (e.g., porosity $\theta_{sat} = 0.39\,\mathrm{m^3\,m^{-3}}$) and a range of saturated hydraulic conductivity (K_{sat}) values, did not produce any overland flow. When θ_{sat} or the value of K_{sat} at the seepage face ($K_{sat,\,sf}$) were reduced, it was possible to produce overland flow, and this result informed the design of sensitivity experiments to test two hypotheses: that the soil is homogeneous, and that the soil has developed some heterogeneity in the downstream direction due to saturated soil compaction near the seepage face. We then performed over 20 000 simulations seeking the optimal parameters to reproduce measured seepage face outflow and hillslope water storage. In these sensitivity simulations we varied $K_{\text{sat, sf}}$, K_{sat} in the upslope soil, and θ_{sat}. We also considered two values of the pore size distribution parameter (n), obtained from a particle size distribution analysis ($n = 2.26$) and by laboratory fitting of the van Genuchten relationship for the LEO soil ($n = 1.72$). The optimized values for n (2.26) and for upslope K_{sat} (1.4×10^{-4} m s^{-1}) are higher than the values measured in the laboratory ($n = 1.72$ and $K_{\text{sat}} \sim 1.9 - 2.5 \times 10^{-5}$ m s^{-1}). For both n values, we obtained that (1) simulations with $K_{\text{sat, sf}} < K_{\text{sat}}$ (heterogeneity hypothesis) produced a higher probability of best realizations than those with $K_{\text{sat, sf}} = K_{\text{sat}}$ (homogeneity hypothesis) and (2) the best realizations with the heterogeneous soil yielded smaller errors than those with the homogeneous soil. The modeling results thus support the hypothesis of localized heterogeneity due to downslope compaction of the LEO soil. A possible mechanism for the compaction could be fine sediments transported during subsurface saturated flow prior to the onset of overland flow.

The suggested hypothesis and the mechanisms for it nonetheless require further investigation. The seepage face in LEO was designed to facilitate downslope flow and consists of a 0.5 m wide gravel section held in place by a plastic plate perforated with 2 mm holes. Shortly after the experiment we removed the gravel to a depth of 72 cm and determined the fraction of fines. According to these observations the amount of fines per volume of gravel is insignificant (~ 2 %) and thus unlikely to cause a reduction in hydraulic conductivity of the seepage face compared to the LEO soil. We did however observe some of the holes in the plate to be clogged with fines, but were unable to test the effect of this clogging on the hydraulic conductivity of the seepage face. Also the observations were not taken over the entire 1 m depth of the seepage face. Further research involving detailed analysis of soil moisture and water potential is ongoing to address the nature and extent of any emergent heterogeneity at LEO.

HESSD
10, 12615–12641, 2013

Concerning the value of the pore size distribution index suggested by the simulation results, it may be that a higher value is justified for the large volume of LEO (334.5 m^3) compared to the volume of the cores in the laboratory. In situ measurements of volumetric water content (with 5TM Decagon probes) and pore water pressure (with MPS-2 Decagon probes) indicate that higher n values are not unrealistic for the LEO soil (see Fig. 4). There is however significant uncertainty in these measurements due to sensor inaccuracy (the pore water pressure sensors became saturated at levels above –6 kPa, making them ineffective for wet conditions).

References

Camporese, M., Paniconi, C., Putti, M., and Orlandini, S.: Surface-subsurface flow modeling with path-based runoff routing, boundary condition-based coupling, and assimilation of multisource observation data, Water Resour. Res., 46, W02512, doi:10.1029/2008WR007536, 2010.

Dontsova, K., Steefel, C. I., Desilets, S., Thompson, A., and Chorover, J.: Solid phase evolution in the Biosphere 2 hillslope experiment as predicted by modeling of hydrologic and geochemical fluxes, Hydrol. Earth Syst. Sci., 13, 2273–2286, doi:10.5194/hess-13-2273-2009, 2009.

Gevaert, A., Teuling, A. J., Uijlenhoet, R., and Troch, P. A.: Hillslope experiment demonstrates role of convergence during two-step saturation, Geophys. Res. Lett., submitted, 2013.

Hernandez, C. M. and Schaap, M. G.: Hydrology simulations on basalt soil for the Landscape Evolution Observatory (LEO), Abstract No. H53I-1644, AGU Fall Meeting, 3–7 December 2012, San Francisco, 2012.

Hopp, L., Harman, C., Desilets, S. L. E., Graham, C. B., McDonnell, J. J., and Troch, P. A.: Hillslope hydrology under glass: confronting fundamental questions of soil-water-biota coevolution at Biosphere 2, Hydrol. Earth Syst. Sci., 13, 2105–2118, doi:10.5194/hess-13-2105-2009, 2009.

Huxman, T., Troch, P. A., Chorover, J., Breshears, D. D., Saleska, S., Pelletier, J., Zeng, X., and Espeleta, J.: The hills are alive: interdisciplinary Earth science at biosphere 2, EOS, 90, p. 120, 2009.

Ivanov, V. Y., Fatichi, S., Jenerette, G. D., Espeleta, J. F., Troch, P. A., and Huxman, T. E.: Hysteresis of soil moisture spatial heterogeneity and the “homogenizing” effect of vegetation, Water Resour. Res., 46, W09521, doi:10.1029/2009WR008611, 2010.

HESSD
10, 12615–12641, 2013

Title Page
Abstract | Introduction
Conclusions | References
Tables | Figures
◂I | I▸
◂ | ▸
Back | Close
Full Screen / Esc
Printer-friendly Version
Interactive Discussion

Table 1. Model scenarios and associated parameter values.

	M1	M2	M3_Homo	M3_Hetero	M4_Homo	M4_Hetero
van Genuchten n (–)	2.26	2.26	1.72	1.72	2.26	2.26
Saturated matric potential ψ_{sat} (m)	−0.48	−0.48	−0.6	−0.6	−0.6	−0.6
Residual moisture θ_r ($m^3\,m^{-3}$)	0.035	0.035	0.002	0.002	0.002	0.002
Specific storage S_s (–)	5.0×10^{-4}	5.0×10^{-4}	5.0×10^{-4}	5.0×10^{-4}	5.0×10^{-4}	5.0×10^{-4}
Porosity θ_{sat} ($m^3\,m^{-3}$)	0.39	0.39	21 values from 0.33 → 0.38			
Saturated hydraulic conductivity K_{sat} ($10^{-5}\,m\,s^{-1}$)	0.78	380	30 values from 1 → 30			
K_{sat} at the seepage face $K_{sat,\,sf}$ ($10^{-5}\,m\,s^{-1}$)	0.78	380	K_{sat}	18 values 1.4 → 3.1	K_{sat}	18 values 1.4 → 3.1
Total number of simulations	1	1	21 × 30 = 630	21 × 30 × 18 = 11 340	21 × 30 = 630	21 × 30 × 18 = 11 340

HESSD
10, 12615–12641, 2013

Analysis of an extreme rainfall-runoff event at the LEO

G.-Y. Niu et al.

HESSD
10, 12615–12641, 2013

Table 2. Optimized parameter values for K_{sat}, $K_{sat,\,sf}$, and θ_{sat} and mean relative errors (e; %).

	M3_Homo	M3_Hetero	M4_Homo	M4_Hetero
n (–)	1.72	1.72	2.26	2.26
θ_{sat} ($m^3\,m^{-3}$)	0.3625	0.3625	0.370	0.3675
K_{sat} ($m\,s^{-1}$)	1.2×10^{-4}	1.7×10^{-4}	1.0×10^{-4}	1.4×10^{-4}
$K_{sat,\,sf}$ (ms^{-1})	1.2×10^{-4}	2.3×10^{-5}	1.0×10^{-4}	2.2×10^{-5}
e (%)	12.99	10.74	8.40	7.38

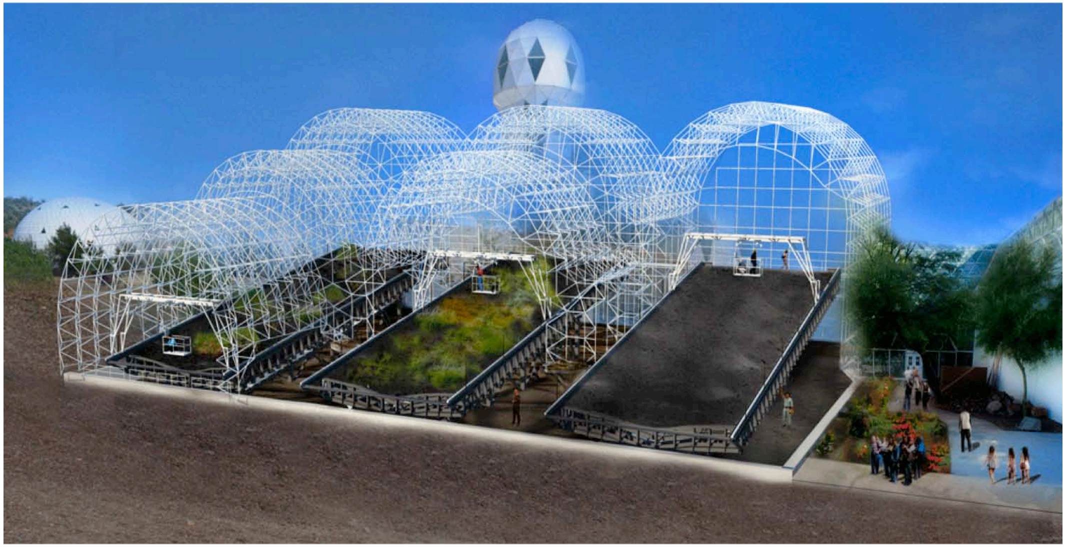

Fig. 1. Diagram showing the three identical convergent landscapes (30 m long and 11.15 m wide) of the Biosphere 2 Landscape Evolution Observatory (LEO) constructed with embedded load cells inside an environmentally controlled greenhouse facility.

HESSD
10, 12615–12641, 2013

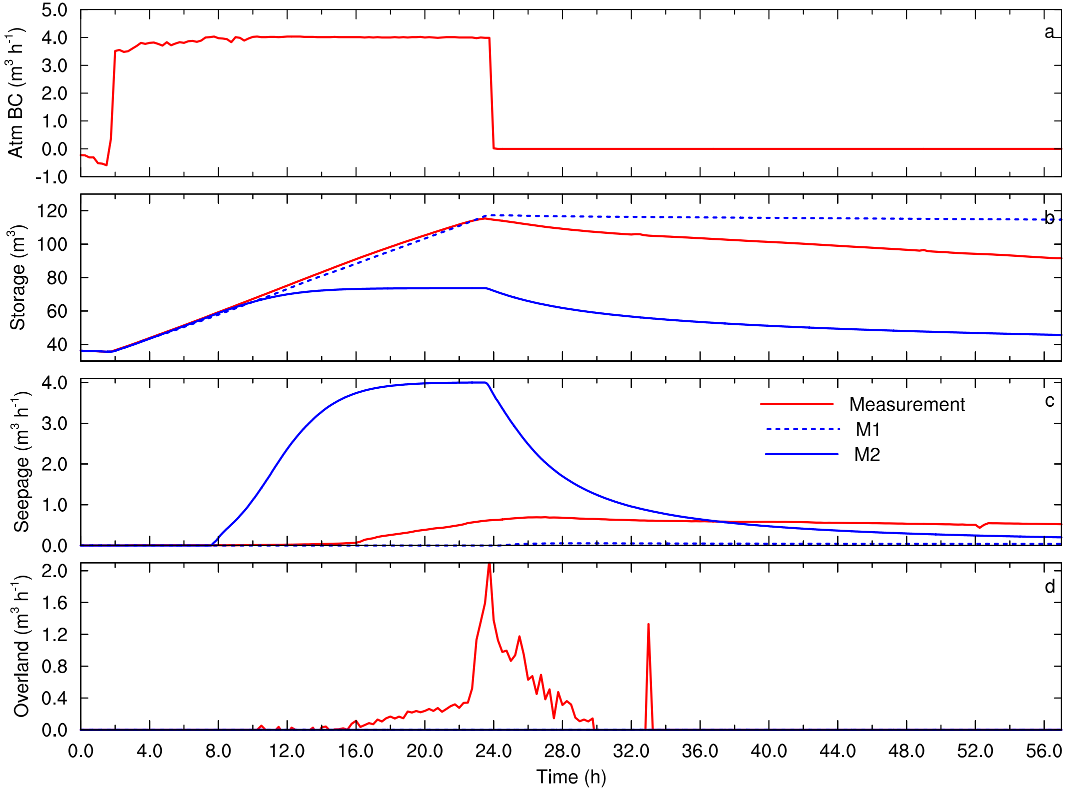

Fig. 2. Comparison between the measured data and the modeling results from scenarios M1 and M2. From the top panel to the bottom are the atmospheric boundary conditions ($m^3\,h^{-1}$), total water storage (m^3), seepage face flow ($m^3\,h^{-1}$), and overland flow ($m^3\,h^{-1}$).

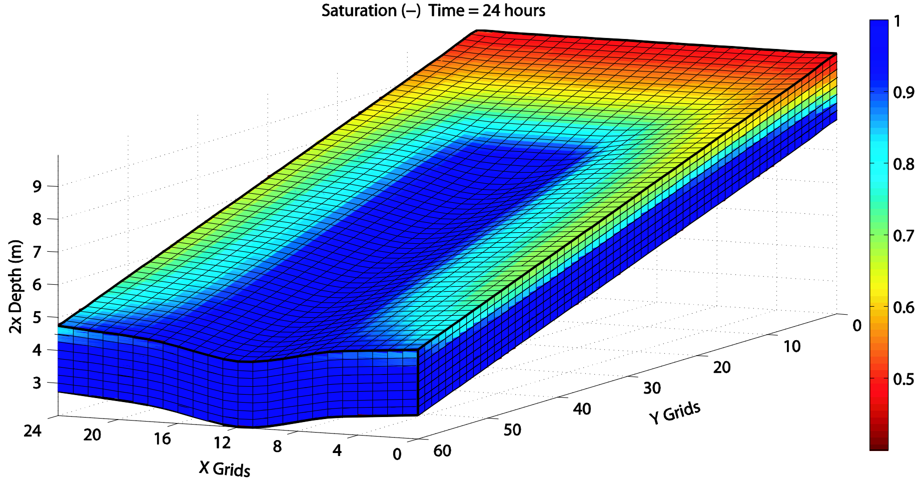

Fig. 3. Discretization of the LEO soil with 60 × 24 × 8 grid cells and 61 × 25 × 9 nodes (the vertical depth of soil is exaggerated by a factor of 2). Color indicates the modeled degree of saturation at time 24 h of the best realization ($n = 2.26$ in Fig. 9).

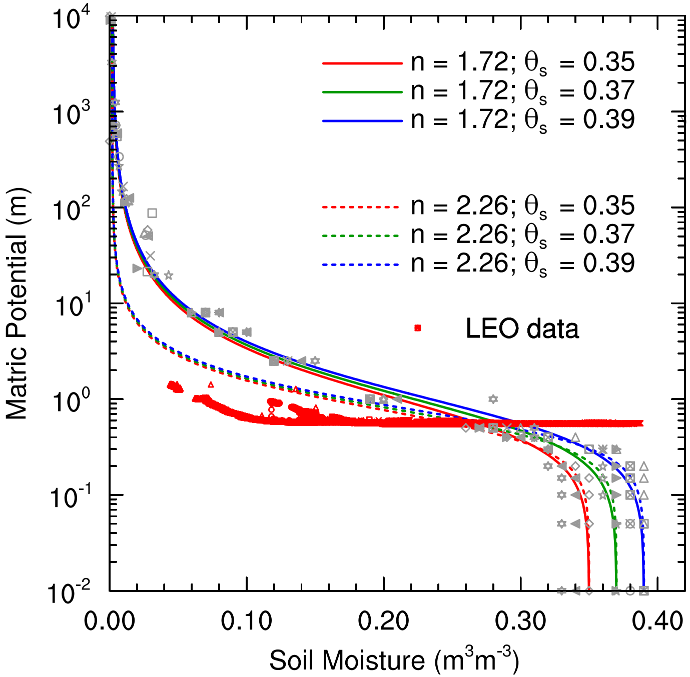

Fig. 4. The relationship between soil moisture and matric potential from laboratory experiments (the grey markers represent different sampling depths) and from the van Genuchten fitting curves for different porosities. The solid curves attempt to match the laboratory data with $n = 1.72$ while the dashed curves are from a particle size distribution analysis and match better the in situ LEO data (red symbols) with $n = 2.26$.

HESSD
10, 12615–12641, 2013

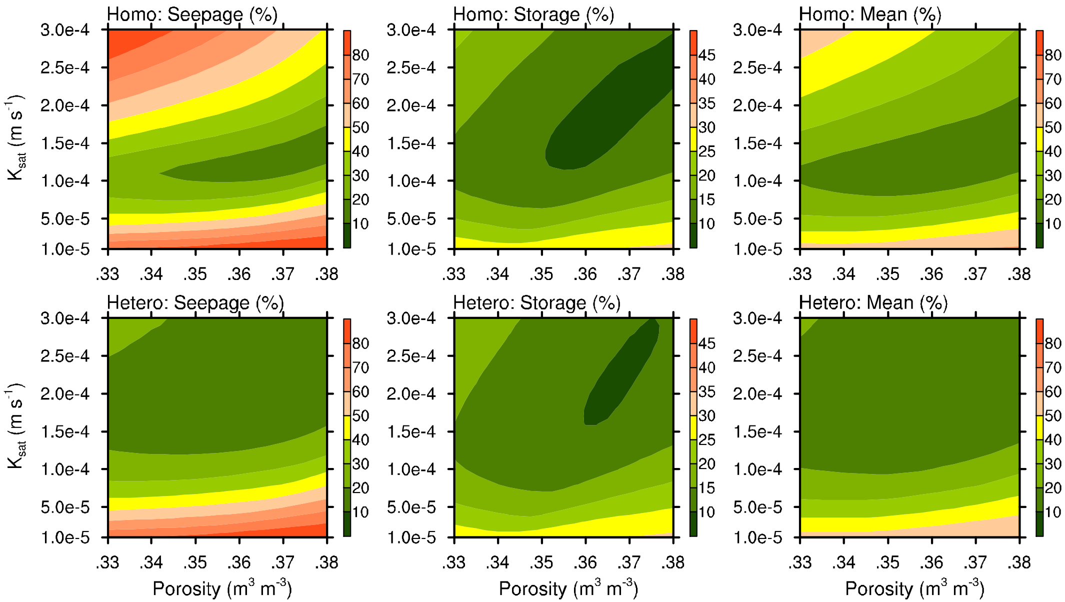

Fig. 5. Relative model error (e) of seepage flow and water storage and the mean error for M3_Homo (upper panel) and M3_Hetero (lower panel; with $K_{sat,\,sf} = 2.1 \times 10^{-5}\,\mathrm{m\,s^{-1}}$) over the parameter space of K_{sat} and porosity.

HESSD
10, 12615–12641, 2013

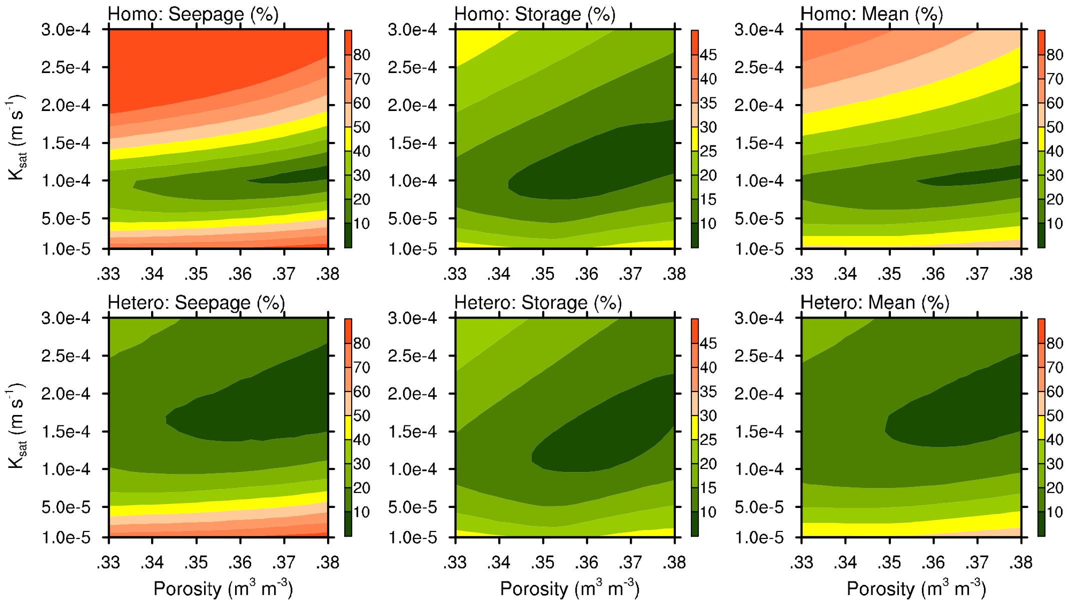

Fig. 6. Relative model error (e) of seepage flow and water storage and the mean error for M4_Homo (upper panel) and M4_Hetero (lower panel; with $K_{sat,\,sf} = 1.9 \times 10^{-5}\,m\,s^{-1}$) over the parameter space of K_{sat} and porosity.

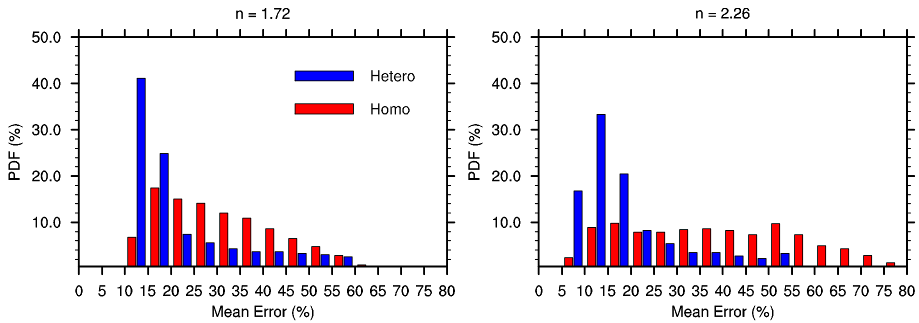

Fig. 7. Probability density functions of the mean error for M3 ($n = 1.72$) and M4 ($n = 2.26$). The results for M3_Hetero and M4_Hetero are obtained with the optimized $K_{\text{sat, sf}}$ values used in Figs. 5 and 6, i.e., $2.1 \times 10^{-5}\,\text{m}\,\text{s}^{-1}$ and $1.9 \times 10^{-5}\,\text{m}\,\text{s}^{-1}$, respectively.

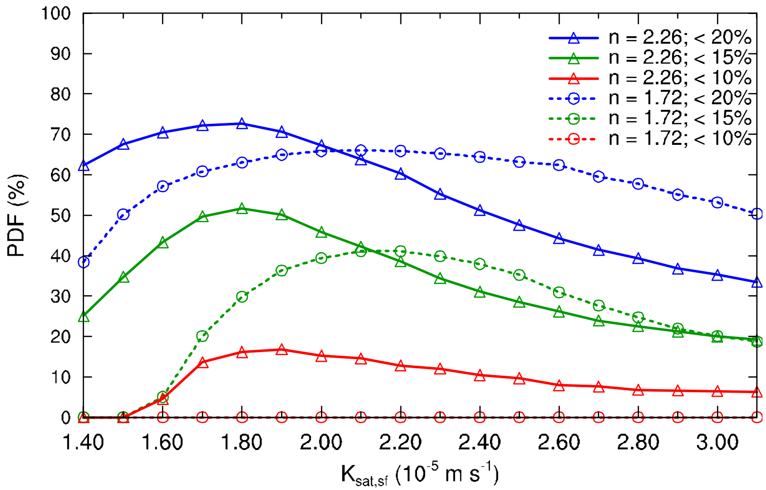

Fig. 8. Probability density functions of the mean error for M3_Hetero ($n = 1.72$) and M4_Hetero ($n = 2.26$) simulations at various error levels across the 18 $K_{\mathrm{sat,\ sf}}$ values considered.

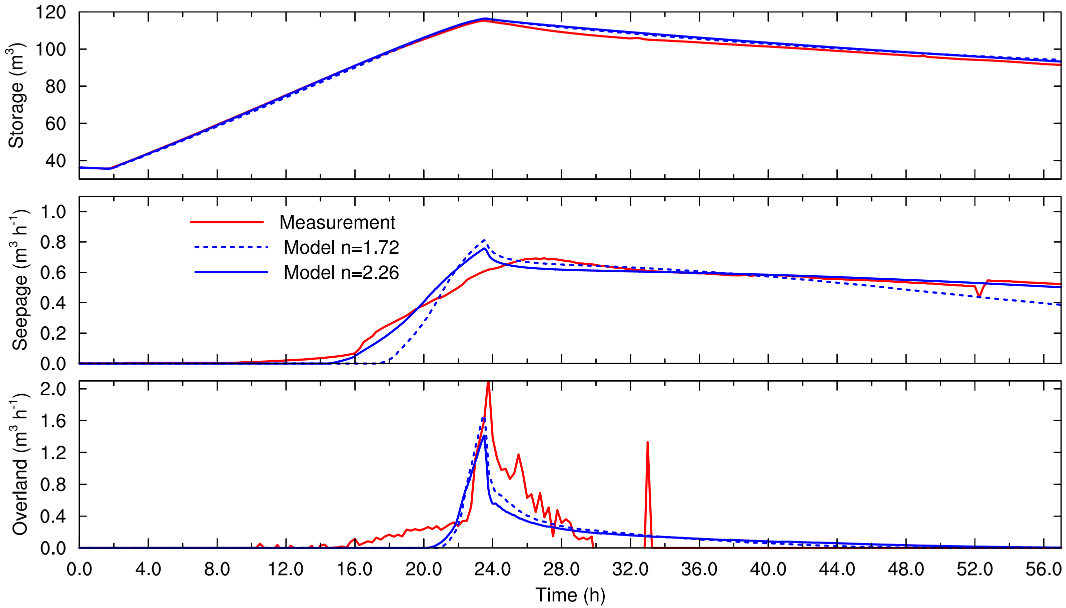

Fig. 9. Comparison between the measured total water storage (top panel), seepage face flow (middle panel), and overland flow (bottom panel) and the simulated results obtained with the optimized parameter values for M3_Hetero ($n = 1.72$) and M4_Hetero ($n = 2.26$).

HESSD
10, 12615–12641, 2013